# Effect of chloride and sulfate ions in simulated boiler water on pitting corrosion behavior of 13Cr steel

Li-Bin Niu [a, *], Kensuke Nakada [b]

[a] Institute of Engineering, Academic Assembly, Shinshu University, 4-17-1 Wakasato, Nagano 380-8553, Japan

[b] Graduate student, Shinshu University. Present: Nachi-Fujikoshi Corp., 1-1-1 Fujikoshi-Honmachi, Toyama 930-8511, Japan

* Corresponding author.

Tel.: +81-26-269-5520. E-mail address: niulibn@shinshu-u.ac.jp.

Abstract

The pitting corrosion behavior of 13Cr steel was investigated in simulated boiler waters containing chloride ions ($Cl^-$) and sulfate ions ($SO_4^{2-}$) using potentiodynamic and potentiostatic polarization tests in addition to pit morphology analysis. The presence of 100 ppm $Cl^-$ in the water caused pitting corrosion of the steel. Pit initiation was inhibited by the addition of 50 ppm or 100 ppm $SO_4^{2-}$ into the water containing 100 ppm $Cl^-$. Pit growth was also suppressed by the presence of 50 ppm $SO_4^{2-}$ in the water with 100 ppm $Cl^-$; however, it was conversely promoted in the presence of 100 ppm $SO_4^{2-}$.

*Keywords:*

A. Stainless steel

B. Polarization

B. SEM

C. Pitting corrosion

## 1. Introduction

In low-pressure (LP) steam turbines of power plants, trace amounts of corrosive chemicals such as chloride ions ($Cl^-$) and sulfate ions ($SO_4^{2-}$) present in the steam are easily concentrated in condensed water droplets and accumulate inside gap regions in the vicinity of the phase transition zone (PTZ) due to the alternating dry-wet conditions [1-3]. Thereby, LP steam turbine materials are subject to pitting corrosion and subsequent corrosion, such as corrosion fatigue (CF) and stress corrosion cracking (SCC) [4-6]. For this reason, the effects of these impurity ions on the corrosion of steam turbine materials have been widely investigated to date. It has been made clear that $Cl^-$ has the most pronounced effect on the susceptibility of a material to SCC and pitting, and that $SO_4^{2-}$ promotes the general corrosion of low-alloy steels, especially the rotor materials [7-10]. We have previously reported [10] the pitting corrosion susceptibility of 13Cr stainless steel, which is used for LP steam turbine blades, in environments containing $Cl^-$ and $SO_4^{2-}$, and it was found that the presence of $SO_4^{2-}$ in the test water with $Cl^-$ has an inhibiting effect on the initiation of corrosion pits, but also an accelerating effect on pit growth.

It is well known that $Cl^-$ not only destroys the passive film of stainless steels and leads to the occurrence of pitting corrosion, but also promotes the growth of pitting corrosion due to the concentration of $Cl^-$ inside the pit. On the other hand, it has long been known that $SO_4^{2-}$ has an inhibitory effect on the pitting corrosion of stainless steels [11]. However, there are still many unknown factors regarding the relationship between the initiation and growth mechanisms of

pitting corrosion on stainless steels and these impurity ions. Furthermore, the combined effects of $Cl^-$ and $SO_4^{2-}$ on the pitting corrosion behavior of 13Cr steel used for LP steam turbine blades has not yet been clarified. In this work, the effect of $Cl^-$ and $SO_4^{2-}$ in simulated boiler water on the initiation and growth behavior of corrosion pits in 13Cr steel was evaluated by anodic polarization tests and pit morphology analyses.

## 2. Experimental

### 2.1. Material and specimens

The test material was 13Cr stainless steel with a chemical composition (mass%) of 0.21 C, 0.32 Si, 0.62 Mn, 13.36 Cr, 0.46 Ni, and the balance of Fe. The 13Cr stainless steel has a heat treatment history of oil-quenching from 980 °C followed by tempering at 670 °C for 3 h and then at 640 °C for 3 h, which produces a tempered martensitic microstructure with no coarse carbide on the prior austenite grain boundaries. This steel has been used as the blade material for LP steam turbines of thermal power plants. Specimens with a size of 25×15×2 $mm^3$ were cut from virgin steam turbine materials. The surfaces were abraded using 150-600 grit emery papers. Prior to testing, the specimens were degreased with acetone and rinsed with deionized pure water. For the anodic polarization tests, the specimens were isolation-treated by coating a liquid type RTV rubber on the surfaces, leaving a reaction area of 1 $cm^2$ exposed to the test water.

## 2.2. Test water

In thermal power plants, various water treatments such as all volatile treatment (AVT) and oxygenated treatment (OT) are typically applied to prevent corrosion and restrain scaling in the water-steam cycles. In this work, AVT water (pH 9.5, dissolved oxygen (DO) < 7 ppb) was simulated on the base of JIS B 8223 [12] with ion-exchanged pure water. The pH value was adjusted by injecting 25% ammonia solution into the water. The removal of DO was performed by continuously bubbling with $N_2$ gas from 1 h before the test and during the test, and also by the addition of 10 ppb hydrazine ($N_2H_4$). Three types of test water were prepared by the addition of 100 ppm $Cl^-$ to the simulated AVT water, and then with the addition of 0 ppm ($SO_4^{2-}$-free), 50 ppm, and 100 ppm of $SO_4^{2-}$, respectively. Table 1 shows the quality of the test waters. $Cl^-$ and $SO_4^{2-}$ were added as powdered NaCl and $Na_2SO_4$, respectively. It should be noted that sodium ions ($Na^+$) have been confirmed to have almost no influence on the corrosion behavior of the steam turbine material [8,9]. The temperature of the test waters was 90 °C.

## 2.3. Electrochemical corrosion test

The anodic polarization tests were conducted using a potentiostat (Hokuto-Denko, HZ-3000) with three electrodes; the specimen as the working electrode, a platinum counter electrode, and a saturated KCl-Ag/AgCl reference electrode. Prior to testing, the specimens were cathodically processed for 10 min at -1.0 V (vs. Ag/AgCl) in the test waters to remove the oxide film on the surface.

Potentiodynamic polarization tests of the specimens were conducted in the test waters with a scan rate of 20 mV/min in the anodic direction until the current density reached 1000 μA/cm$^2$. The metastable pitting potential $V_m$ [13,14], which corresponds to the first current peak in the passive region, and the potentials at which the current density reached 10 μA/cm$^2$ $V'_{c10}$, were recorded from the potentiodynamic polarization curves. $V'_{c10}$ has sometimes been used as an approximation of the pitting potential [15]. After the potentiodynamic polarization tests, the specimens were examined using a digital camera and an optical microscope (OM).

Potentiostatic polarization tests of the specimens were then conducted for 20 h in the three test waters. The applied potentials were the $V'_{c10}$ potentials of the specimens obtained in the $SO_4^{2-}$-free test water with only 100 ppm $Cl^-$ added and in that with both 100 ppm $Cl^-$ and 100 ppm $SO_4^{2-}$. After the potentiostatic polarization tests, the specimen surfaces were observed with a digital camera, an OM, and a scanning electron microscope (SEM). SEM observations and elemental analyses with energy-dispersive X-ray spectroscopy (EDS) were also conducted on cross-sections of the pits found on the specimens. The cross-sections of the pits were the emery-abraded cutting planes, which did not always pass through the pit centers because they were very small. For the EDS analyses, elemental mapping was performed on the entire cross-section, while point analysis was performed on the pit wall or the product inside the pit. The specimens for EDS analysis were embedded in resin and were Au-sputtering treated, so that C and Au from this process were also detected in the EDS results.

## 3. Results and discussion

### 3.1. Potentiodynamic polarization behavior

Fig. 1 shows potentiodynamic polarization curves for 13Cr steel in the test waters at 90 °C. For the specimen in the $SO_4^{2-}$-free test water with only 100 ppm $Cl^-$, current transients caused by the initiation and repassivation of metastable pitting are evident from a lower potential of about 0.07 V (vs. Ag/AgCl) in the passive region [16,17]. The metastable pitting potentials $V_m$, and the $V'_{c10}$ potentials of 13Cr steel obtained from the potentiodynamic polarization tests are shown in Fig. 2. Both $V_m$ and $V'_{c10}$ were lowest in the $SO_4^{2-}$-free test water, while they shifted to noble values in the two test waters with added $SO_4^{2-}$ and increased with the $SO_4^{2-}$ concentration. Recently, Tang et al. [14] reported that a good linear relationship exists between the metastable pitting potential and the pitting potential, which is similar to that observed in the present work.

Fig. 3 shows the appearance of the specimens after the potentiodynamic polarization tests. Pitting corrosion occurred on all the specimens and a large amount of pits was observed on the specimen from the $SO_4^{2-}$-free simulated AVT water with only 100 ppm $Cl^-$. Fig. 4 shows the number density of pits measured by OM observations of the specimens. The number density was significantly decreased with the addition of $SO_4^{2-}$ into the simulated AVT water containing 100 ppm $Cl^-$, even though it was slightly larger in the water with 100 ppm $SO_4^{2-}$ than in that with 50 ppm $SO_4^{2-}$. This behavior is in agreement with the results shown in Fig. 2, in which both the $V_m$ and $V'_{c10}$ potentials increased with the addition of $SO_4^{2-}$ to the test water. These results suggest that pit initiation on

13Cr steel was inhibited by the presence of $SO_4^{2-}$ in the AVT boiler water containing 100 ppm $Cl^-$.

$Cl^-$ ions are well known to be aggressively destructive toward passive film and cause pitting corrosion on stainless steels. It has been reported that the presence of $SO_4^{2-}$ in a solution containing $Cl^-$ ennobles the pitting potential and has the effect of suppressing the pitting corrosion of stainless steels [11]. Pistorious and Burstein [17] suggested that the addition of $SO_4^{2-}$ into a solution containing $Cl^-$ lowers the solubility of the protective salt cover (passivation film) formed on the stainless steel surface, which inhibits pitting corrosion. In the present work, it is considered that for 13Cr steel in simulated AVT boiler water with added $Cl^-$, the increase of the metastable/stable pitting potentials and the decrease in the number density of pits due to the addition of $SO_4^{2-}$ is considered to be due to the formation of salt films containing sulfates, such as $FeSO_4$ and $Cr_2(SO_4)_3$, which have relatively low solubility on the specimen surfaces, which inhibit pit initiation.

### 3.2. Potentiostatic polarization behavior

Potentiostatic polarization tests were conducted in the test waters for 20 h at applied potentials of 0.29 V (vs. Ag/AgCl) and 0.37 V (vs. Ag/AgCl). The applied potentials were the $V'_{c10}$ potentials of the specimens obtained from the potentiodynamic polarization tests in AVT water with only 100 ppm $Cl^-$ and in AVT water with both 100 ppm $Cl^-$ and 100 ppm $SO_4^{2-}$, respectively. Fig. 5 shows the time variations of the current density during polarization. At both applied potentials, the anodic current in the specimens in the $SO_4^{2-}$-free water increased

to higher values. It is considered that pitting corrosion continued to initiate and proceed stably for the 13Cr steel in the AVT boiler water containing only 100 ppm $Cl^-$. On the other hand, in the other two test waters with added $SO_4^{2-}$, the anodic current decreased, even though the values were larger just after the start of test. It is presumed that pitting corrosion on the specimen surfaces progressed with repeated pit initiation and repassivation in the two test waters. Furthermore, as shown in Fig. 5(a), at 0.29 V (vs. Ag/AgCl), the anodic current decreased in proportion to the increase in the concentration of $SO_4^{2-}$ added, and current oscillations dwindled down after approximately 10 h from the start of the test. However, at 0.37 V (vs. Ag/AgCl), as shown in Fig. 5(b), the anodic current in the test water with 100 ppm $SO_4^{2-}$ was larger than that in the test water with 50 ppm $SO_4^{2-}$, and it increased rapidly after approximately 19 h of testing.

Figs. 6 and 7 show the appearance of the specimens after the potentiostatic polarization tests at 0.29 V (vs. Ag/AgCl) and 0.37 V (vs. Ag/AgCl), respectively. For the specimens tested at 0.29 V (vs. Ag/AgCl) (Fig. 6), it is estimated that the pitting corrosion grew stably in the $SO_4^{2-}$-free AVT water because more corrosion products were observed around the pits than on the specimens tested in the waters with added $SO_4^{2-}$. In addition, it is considered that the corrosion products were composed mainly of Fe-oxides such as $Fe(OH)_2$ and $Fe_3O_4$. For the specimens tested at 0.37 V (vs. Ag/AgCl) (Fig. 7), the progression of pitting corrosion was evident in all the test waters. Fig. 8 gives the number density of pits on the specimen surfaces. At both applied potentials, smaller number densities of pits were confirmed on the specimens tested in the $SO_4^{2-}$-free test water than those in the test waters with added $SO_4^{2-}$. This is opposite to the

pitting number density results obtained in the potentiodynamic polarization tests (Fig. 4).

Firstly, potentiostatic polarization behavior of the specimens at 0.29 V (vs. Ag/AgCl) is discussed. The applied potential was $V'_{c10}$ (the approximate pitting potential) for 13Cr steel in the $SO_4^{2-}$-free test water; therefore, it is considered that once pitting is initiated on the specimen during polarization under such conditions, it will proceed stably. A small number of pits was initiated in the $SO_4^{2-}$-free water; therefore, it is presumed that the stable increase of current density shown in Fig. 5(a) is mainly due to pit growth. In contrast, as shown in Fig. 1, the applied potential of 0.29 V (vs. Ag/AgCl) was also in the passive regions and below the $V'_{c10}$ potentials in the two waters with added $SO_4^{2-}$. It is thus considered that for the specimens during polarization at the $V'_{c10}$ potential in the two test waters with added $SO_4^{2-}$, metastable pits are initiated on the specimens but are repassivated and do not grow larger. It is suggested that the decrease of current density in the two test waters shown in Fig. 5(a) is due to repassivation of the pitting. Burstein et al. [18] reported that once the sites on a specimen are activated and repassivated, they are no longer available for further pitting. For the same reason, in the present polarization tests at 0.29 V (vs. Ag/AgCl) using the two test waters with added $SO_4^{2-}$, new metastable pits were repeatedly initiated and repassivated one after another at discrete sites, so that a large number of pits were observed on the specimen surfaces, as shown in Fig. 8.

Next, the potentiostatic polarization behavior of the specimens at 0.37 V (vs. Ag/AgCl) is discussed. It is presumed that in the $SO_4^{2-}$-free test water, the tendency of the current density to increase shown in Fig. 5(b) can be attributed

mainly to pit growth, in the same way as that at 0.29 V (vs. Ag/AgCl). In the other two test waters with added $SO_4^{2-}$, pit growth was suppressed and the current density decreased, although a large number of pits were initiated. Pistorious and Burstein [17] suggested that the suppression of pit growth due to the addition of $SO_4^{2-}$ is due to the formation of a salt film with lower solubility that covers over the pit mouth and serves as a barrier to the diffusion of metal cations. On the other hand, as shown in Fig. 5(b), the specimen in the test water with 100 ppm $SO_4^{2-}$ exhibited a larger current density than that in the test water with 50 ppm $SO_4^{2-}$ added, even though a relatively small number of pits were initiated on the specimen (Fig. 8). Therefore, although the applied potential of 0.37 V (vs. Ag/AgCl) was higher than the $V'_{c10}$ potential in the water with 50 ppm $SO_4^{2-}$ added, the pit growth rate was lower than that in the water with 100 ppm $SO_4^{2-}$. This phenomenon suggests that pit growth was conversely promoted by the addition of a large amount of $SO_4^{2-}$.

### 3.3. Pit growth behavior

The effect of $SO_4^{2-}$ addition on the pit growth behavior of 13Cr steel in simulated AVT boiler water containing 100 ppm $Cl^-$ was investigated using the specimens from the potentiostatic polarization tests. Figs. 9 and 10 show SEM micrographs of typical pits on the specimens after the potentiostatic polarization tests at 0.29 V (vs. Ag/AgCl) and 0.37 V (vs. Ag/AgCl), respectively. Many of the pits on the specimens tested at both applied potentials in the $SO_4^{2-}$-free test water (Fig. 9(a), Fig. 10(a)) and those tested at 0.37 V (vs. Ag/AgCl) in the water with 100 ppm $SO_4^{2-}$ (Fig. 10(c)) were larger with open pit mouths. On the other

hand, most of the pits on the specimens tested at 0.29 V (vs. Ag/AgCl) in the two test waters with added $SO_4^{2-}$ and those tested at 0.37 V (vs. Ag/AgCl) in the water with 50 ppm $SO_4^{2-}$ exhibited morphology where pit mouths were covered. Fig. 11 shows SEM micrographs of pit cross-sections on the specimen surfaces after the potentiostatic polarization tests at 0.29 V (vs. Ag/AgCl). As shown in Fig. 11(a), the pit produced in the $SO_4^{2-}$-free test water was larger than the pits grown in test water with added $SO_4^{2-}$, and the pit had an internal shape that was spherical. It is considered that the pit growth was stable in the $SO_4^{2-}$-free test water because there was almost no low solubility salt film formed on the inner surface [19]. In contrast, as shown in high-power magnification cross-sectional SEM images in Figs. 11(b) and (c), the pits produced in the two test waters with added $SO_4^{2-}$ were smaller and the thick salt products were observed inside the pits and covered the pit mouths. It is therefore considered that pit growth during the potentiostatic polarization testing at 0.29 V (vs. Ag/AgCl) in the two test waters with added $SO_4^{2-}$ was suppressed by the salt products inside the pits and covering the pit mouths.

Fig. 12 shows SEM images with elemental mapping results for the cross-sections and Fig. 13 shows EDS spectra for the inner surfaces of the pits on the specimens after the potentiostatic polarization tests at 0.37 V (vs. Ag/AgCl). The SEM micrographs show that for the pit growth in the two test waters with added $SO_4^{2-}$, thick salt films were formed inside the pits or covered the pit mouths. Cracks in the salt films, and gaps between the salt films and the base metal were also clearly observed. In particular, as shown in Fig. 12(c), the pit produced in the test water with 100 ppm $SO_4^{2-}$, the salt cover was cracked open

as it became too thick. The EDS spectrum shown in Fig. 13(a) revealed a large amount of O, Cr, and Fe and a small amount of Cl inside the pit (Fig. 12(a)) produced in the $SO_4^{2-}$-free water. It has been suggested that Cr-oxides (CrOOH, $CrO_3$) and Fe-oxides ($Fe(OH)_2$, $Fe_3O_4$) are formed [20] and $Cl^-$ is concentrated inside such pits. However, a large amount of S was also detected in the salt products inside or covering the pits produced in the two waters with added $SO_4^{2-}$ (Fig. 13(b)); therefore, it is considered that the salt products are a mixture that contains not only Cr-oxides and Fe-oxides, but also sulfates such as $Cr_2(SO_4)_3$ and $FeSO_4$, which have relatively low solubility.

Pistorious and Burstein [17] suggested that at higher potentials, the pit growth is controlled by the diffusion of metal cations, which is dependent on the pit geometry. If a salt cover is formed over the pit mouth, then diffusion will be suppressed and pit growth will be inhibited. However, pit growth will not be suppressed when the cover is destroyed due to the effect of an osmotic pressure difference developing across the pit mouth cover [17,21]. In the present potentiostatic polarization tests conducted in the $SO_4^{2-}$-free test water, because no relatively insoluble product film was significantly formed inside the pits [19], pits growth remained stable. In the two test waters with added $SO_4^{2-}$, salt products with lower solubility were formed on both the inner surfaces of the pits and as covers over the pit mouths; therefore, it is presumed that the pit growth rate was significantly influenced by the solubility of these salt products [22]. Leckie and Uhlig [11] have reported that an increase in the concentration of $SO_4^{2-}$ lowers the solubility of these salt products. However, it has also been reported that the addition of $Na_2SO_4$ to NaCl in solution stabilizes pit growth

[23]. Pit growth will proceed when the salt product pit cover is eliminated and becomes ineffectual as a diffusion barrier [18,24]. In the present potentiostatic polarization tests at 0.37 V (vs. Ag/AgCl), the pit growth rate in the test water with 100 ppm $SO_4^{2-}$ was higher than that in the test water with 50 ppm $SO_4^{2-}$. It is thus considered that pit growth on 13Cr steel in the test water with 100 ppm $SO_4^{2-}$ was promoted by cracking of the salt films formed inside the pits, as well as rupture of the salt covers over the pit mouths because the layer of fragile salt products became too thick. The cracking of these salt films resulted in further pit growth at the gap regions between the salt films and the base metal, while rupture of the salt covers facilitated the diffusion of metal ions.

## 4. Conclusions

(1) The presence of 100 ppm $Cl^-$ in simulated AVT boiler water caused pitting corrosion of 13Cr steel, which is used for LP steam turbine blades.

(2) Pit initiation on 13Cr steel in test water was inhibited by the presence of both $SO_4^{2-}$ with 100 ppm $Cl^-$ because of the protective salt films that are formed and cover the steel surface.

(3) The presence of 50 ppm $SO_4^{2-}$ in simulated AVT boiler water containing 100 ppm $Cl^-$ suppressed pit growth because salt films with lower solubility are formed on the inner surfaces of the pits and as covers over the pit mouths. However, pit growth was conversely promoted with the addition of 100 ppm $SO_4^{2-}$, due to cracking of the salt films inside the pits and rupturing of the salt covers over the pit mouths, which enabled pit growth to continue.

References

[1] Report of Central Research Institute of Electric Power Industry, T97801, Steam chemistry and corrosion in steam turbine, (Tokyo 1998) 29-47.

[2] J. C. Bellows, Chemical processes in steam turbines, PowerPlant Chemistry, 1(1999) 26-30.

[3] B. Dooley, W. P. McNaughton, Recent developments in understanding of the phase transition zone in the low pressure steam turbine, PowerPlant Chemistry, 2(2000) 709-715.

[4] O. Jonas, Steam turbine corrosion, Mater. Perform. 24(1985) 9-18.

[5] O. Jonas, L. Machemer, Steam turbine corrosion and deposits problems and solutions, Proc. 37th Turbomachinery Symposium, (Houston, USA, 2008) 211-228.

[6] Y. Sakai, M. Yamashita, M. Sakata, Geothermal steam turbines with high efficiency, high reliability blades, Geothermal Resources Council Trans. 24(2000) 521-526.

[7] A. Turnbull, S. Zhou, Pit to crack transition in stress corrosion cracking of a steam turbine disc steel, Corros. Sci. 46(2004) 1239-1264.

[8] M. Hirano, Y. Koike, T. Minami, L.-B. Niu, H. Takaku, SCC behavior of low-pressure steam turbine materials for fossil power plants under conditions coexisted with oxygen and corrosive chemicals, Zairyo-to-Kankyo, 53(2004) 568-575.

[9] M. Hirano, S. Itaba, T, Sakurada, Y. Imaizumi, T. Minami, L.-B. Niu, H.

Takaku, Accelerated corrosion behavior due to alternating dry-wet conditions for LP steam turbine materials of fossil power plants, ISIJ Int. 45(2005) 373-379.

[10] L.-B. Niu, T. Goto, T. Nakane, H. Takaku, Y. Sakai, Effect of $Cl^-$ and $SO_4^{2-}$ on pitting corrosion susceptibility for materials of low-pressure steam turbines in power plants, J. Japan Inst. Metals, 74(2010) 635-642.

[11] H. P. Leckie, H. H. Uhlig, Environmental factors affecting the critical potential for pitting in 18-8 stainless steel, J. Electrochem. Soc. 113(1966) 1262-1967.

[12] Japanese Standards Association, Water Conditioning for Boiler Feed Water and Boiler Water; JIS B 8223, (Japanese Standards Association, Tokyo, 2006).

[13] Y. Zuo, H. Wang, J. Zhao, J. Xiong, The effects of some anions on metastable pitting of 316L stainless steel, Corros. Sci. 44(2002) 13-24.

[14] Y. Tang, Y. Zuo, J. Wang, X. Zhao, B. Niu, B. Lin, The metastable pitting potential and its relation to the pitting potential for four materials in chloride solutions, Corros. Sci. 80(2014) 111-119.

[15] Japan Society of Corrosion Engineering, Corrosion Handbook, (Maruzen, Tokyo, 2000) 573-576.

[16] G. S. Frankel, L. Stockert, F. Hunkeler, H. Boehni, Metastable pitting of stainless steel, Corros. 43(1987) 429-436.

[17] P. C. Pistorious, G. T. Burstein, Growth of corrosion pits on stainless steel in chloride solution containing dilute sulphate, Corros. Sci. 33(1992) 1885-1897.

[18] G. T. Burstein, P. C. Pistorius, S. P. Mattin, The nucleation and growth of corrosion pits on stainless steel, Corros. Sci. 35(1993) 57-62.

[19] P. Ernst, R. C. Newman, Pit growth studies in stainless steel foils. Ⅰ.

Introduction and pit growth kinetics, Corros. Sci. 44(2002) 927-941.

[20] L. –B. Niu, H. Kato, K. Shiokawa, K. Nakamura, M. Yamashita, Y. Sakai, Electrochemical crevice corrosion behavior of low-pressure steam turbine materials in the simulated boiler water added chloride and sulfate ions, Mater. Trans. 54(2013) 2225-2232.

[21] J. Mankowski, Z. Szklarska-Smialowska, Studies on accumulation of chloride ions in pits growing during anodic polarization, Corros. Sci. 15(1975) 493-501.

[22] R. C. Alkire, K. P. Wong, The corrosion of single pits on stainless steel in acidic chloride solution, Corros. Sci. 28(1988) 411-421.

[23] P. Ernst, R. C. Newman, Pit growth studies in stainless steel foils. Ⅱ. Effect of temperature, chloride concentration and sulphatr addition, Corros. Sci. 44(2002) 943-954.

[24] P. Ernst, N. J. Laycock, M. H. Moayed, R. C. Newman, The mechanism of lacy cover formation in pitting, Corros. Sci. 39(1997) 1133-1136.

**Figure and Table Captions**

**Fig. 1.** Anodic polarization curves of 13Cr steel in the test waters.

**Fig. 2.** Potential $V'_{c10}$ and metastable pitting potential $V_m$ for 13Cr steel in the test waters.

**Fig. 3.** Appearance of specimens after potentiodynamic polarization in simulated AVT waters with (a) 100 ppm $Cl^-$, (b) 100 ppm $Cl^-$ + 50 ppm $SO_4^{2-}$, and (c) 100 ppm $Cl^-$ + 100 ppm $SO_4^{2-}$.

**Fig. 4.** Number density of pits on the specimens after potentiodynamic polarization tests.

**Fig. 5.** Time variations of current density during potentiostatic polarization at (a) 0.29 V (vs. Ag/AgCl) and (b) 0.37 V (vs. Ag/AgCl).

**Fig. 6.** Appearance of specimens after potentiostatic polarization at 0.29 V (vs. Ag/AgCl) in simulated AVT waters with (a) 100 ppm $Cl^-$, (b) 100 ppm $Cl^-$ + 50 ppm $SO_4^{2-}$, and (c) 100 ppm $Cl^-$ + 100 ppm $SO_4^{2-}$.

**Fig. 7.** Appearance of specimens after potentiostatic polarization at 0.37 V (vs. Ag/AgCl) in simulated AVT waters with (a) 100 ppm $Cl^-$, (b) 100 ppm $Cl^-$ + 50 ppm $SO_4^{2-}$, and (c) 100 ppm $Cl^-$ + 100 ppm $SO_4^{2-}$.

**Fig. 8.** Number density of pits on the specimens after potentiostatic polarization in the test waters for 20 h.

**Fig. 9.** Typical pits on specimens after potentiostatic polarization at 0.29 V (vs. Ag/AgCl) in simulated AVT waters with (a) 100 ppm $Cl^-$, (b) 100 ppm $Cl^-$ + 50 ppm $SO_4^{2-}$, and (c) 100 ppm $Cl^-$ + 100 ppm $SO_4^{2-}$.

**Fig. 10.** Typical pits on specimens after potentiostatic polarization at 0.37 V (vs. Ag/AgCl) in simulated AVT waters with (a) 100 ppm $Cl^-$, (b) 100 ppm $Cl^-$ + 50 ppm $SO_4^{2-}$, and (c) 100 ppm $Cl^-$ + 100 ppm $SO_4^{2-}$.

**Fig. 11.** Cross-sectional SEM images of the pits on specimens after potentiostatic polarization at 0.29 V (vs. Ag/AgCl) in simulated AVT waters with (a) 100 ppm $Cl^-$, (b) 100 ppm $Cl^-$ + 50 ppm $SO_4^{2-}$, and (c) 100 ppm $Cl^-$ + 100 ppm $SO_4^{2-}$.

**Fig. 12.** SEM images and elemental maps of pit cross-sections on specimen surfaces after potentiostatic polarization at 0.37 V (vs. Ag/AgCl) in simulated AVT waters with (a) 100 ppm $Cl^-$, (b) 100 ppm $Cl^-$ + 50 ppm $SO_4^{2-}$, and (c) 100 ppm $Cl^-$ + 100 ppm $SO_4^{2-}$.

**Fig. 13.** EDS spectra for the inner surfaces of pits on specimens after potentiostatic polarization at 0.37 V (vs. Ag/AgCl) in simulated AVT waters with (a) 100 ppm $Cl^-$ and (b) 100 ppm $Cl^-$ + 50 ppm $SO_4^{2-}$. (C and Au detected are due to the Au-sputtering treatment.)

**Table 1**

Quality of the test waters.

Highlights

- The influence of $Cl^-$ and $SO_4^{2-}$ on pitting corrosion behavior was investigated.
- Pit initiation was inhibited by the addition of $SO_4^{2-}$ into the water containing $Cl^-$.
- Pit growth was also suppressed by the presence of 50 ppm $SO_4^{2-}$ with 100 ppm $Cl^-$.
- The addition of 100 ppm $SO_4^{2-}$ with 100 ppm $Cl^-$ promoted pit growth conversely.

**Table 1**
Quality of the test waters.

| Water no. | Impurities | | | Electric Conductivity (mS/m) | pH | DO (ppb) | Temp. (°C) |
|---|---|---|---|---|---|---|---|
| | $Cl^-$ (ppm) | $SO_4^{2-}$ (ppm) | $Na^+$ (ppm) | | | | |
| 1 | 100 | 0 | 65 | 35±1 | 9.5±0.1 | < 7 | 90 |
| 2 | 100 | 50 | 89 | 47±1 | 9.5±0.1 | < 7 | 90 |
| 3 | 100 | 100 | 113 | 60±1 | 9.5±0.1 | < 7 | 90 |

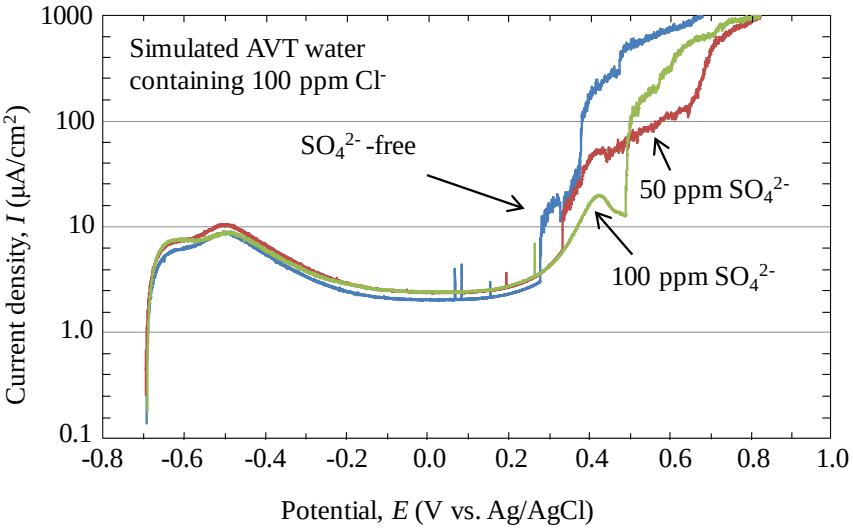


**Fig. 1.** Anodic polarization curves of 13Cr steel in the test waters.

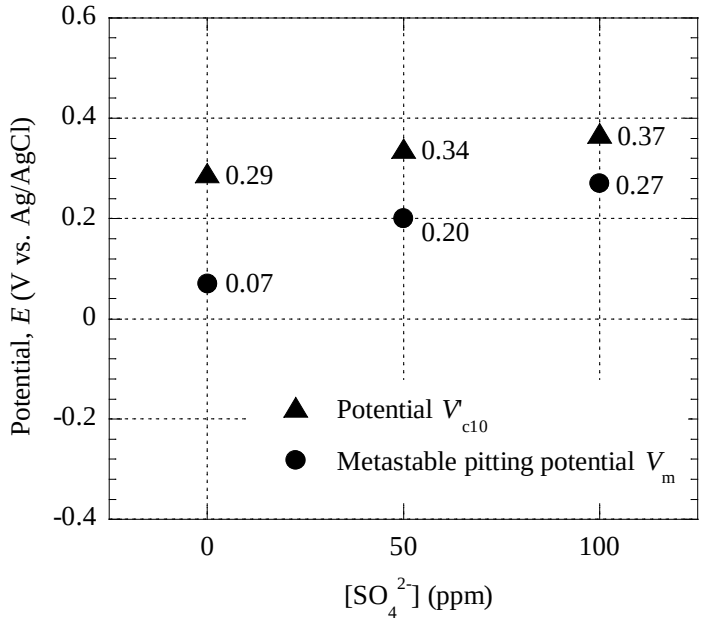


**Fig. 2.** Potential $V'_{c10}$ and metastable pitting potential $V_m$ for 13Cr steel in the test waters.

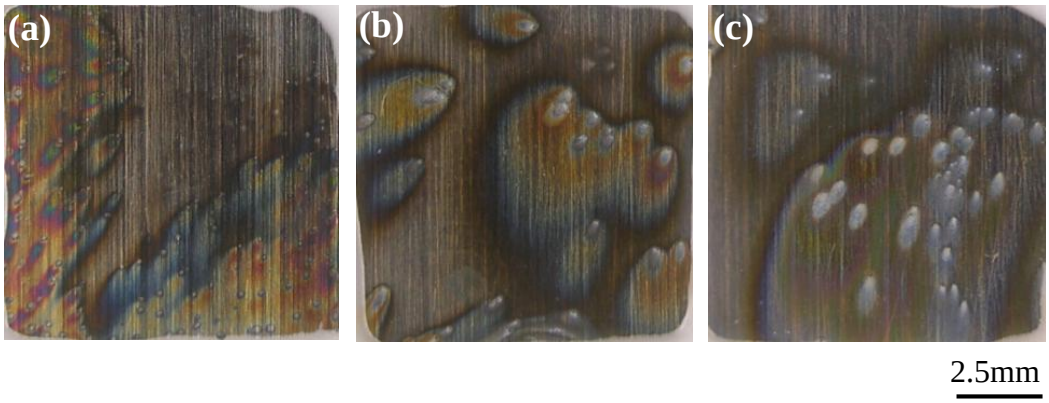


**Fig. 3.** Appearance of specimens after potentiodynamic polarization in simulated AVT waters with (a) 100 ppm $Cl^-$, (b) 100 ppm $Cl^-$ + 50 ppm $SO_4^{2-}$, and (c) 100 ppm $Cl^-$ + 100 ppm $SO_4^{2-}$.

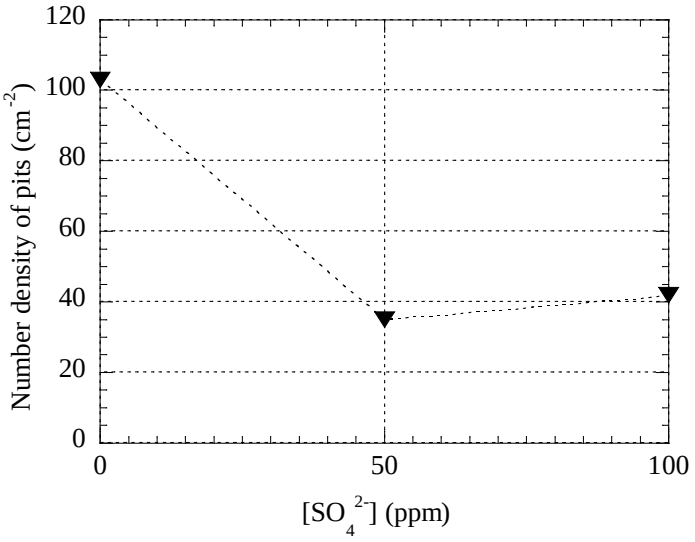


**Fig. 4.** Number density of pits on the specimens after potentiodynamic polarization tests.

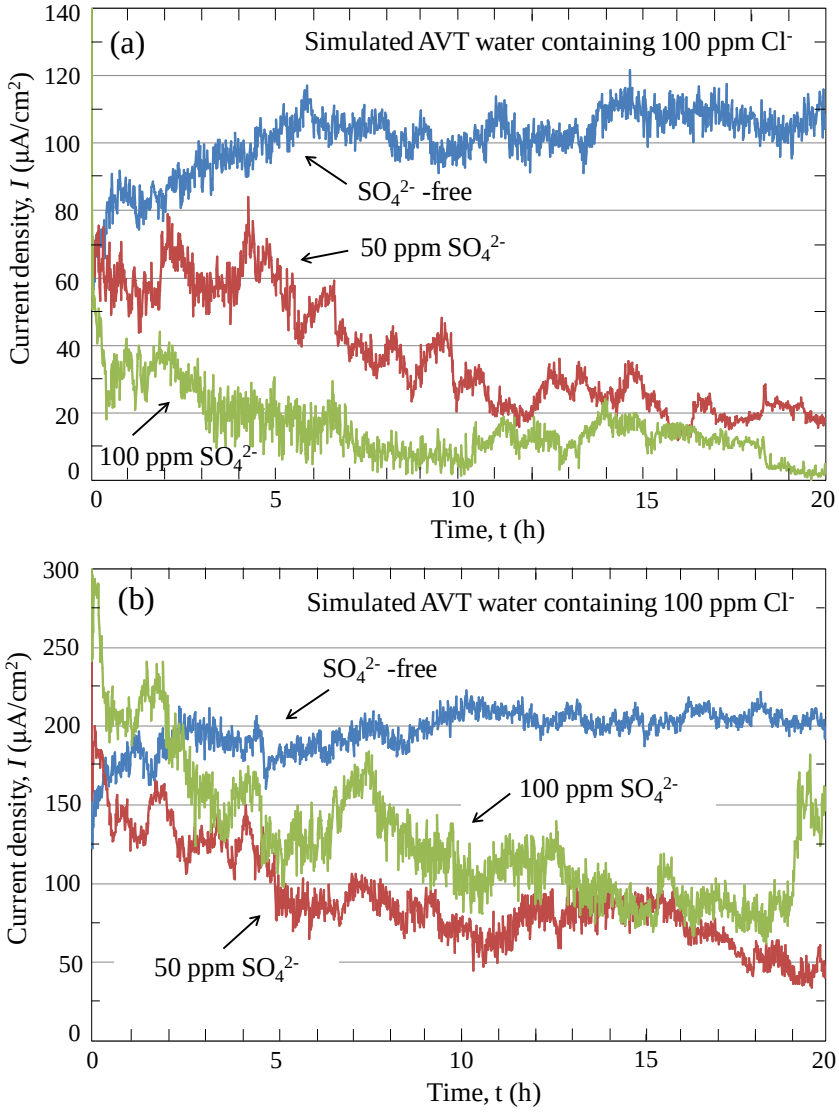


**Fig. 5.** Time variations of current density during potentiostatic polarization at (a) 0.29 V (vs. Ag/AgCl) and (b) 0.37 V (vs. Ag/AgCl).

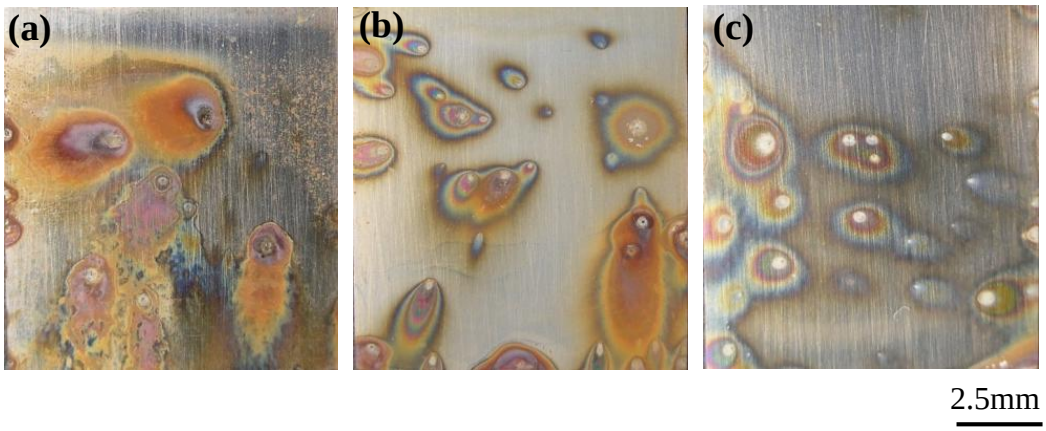


**Fig. 6.** Appearance of specimens after potentiostatic polarization at 0.29 V (vs. Ag/AgCl) in simulated AVT waters with (a) 100 ppm $Cl^-$, (b) 100 ppm $Cl^-$ + 50 ppm $SO_4^{2-}$, and (c) 100 ppm $Cl^-$ + 100 ppm $SO_4^{2-}$.

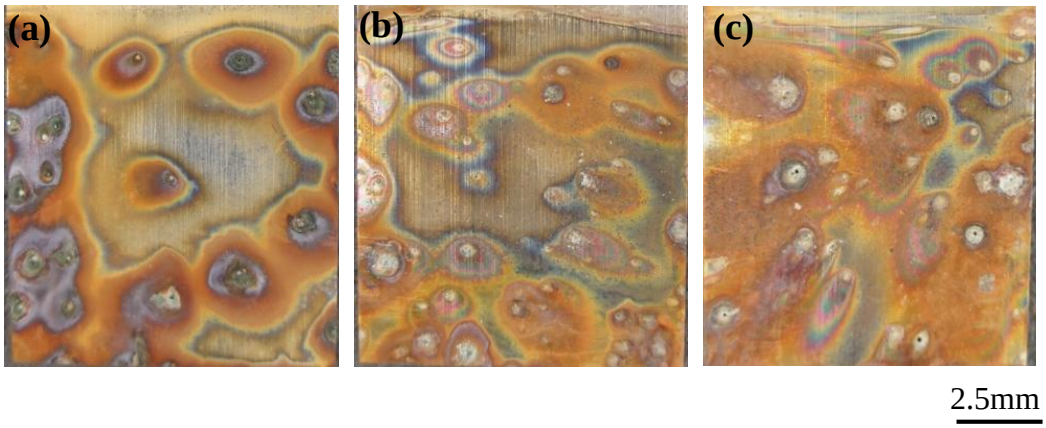


**Fig. 7.** Appearance of specimens after potentiostatic polarization at 0.37 V (vs. Ag/AgCl) in simulated AVT waters with (a) 100 ppm $Cl^-$, (b) 100 ppm $Cl^-$ + 50 ppm $SO_4^{2-}$, and (c) 100 ppm $Cl^-$ + 100 ppm $SO_4^{2-}$.

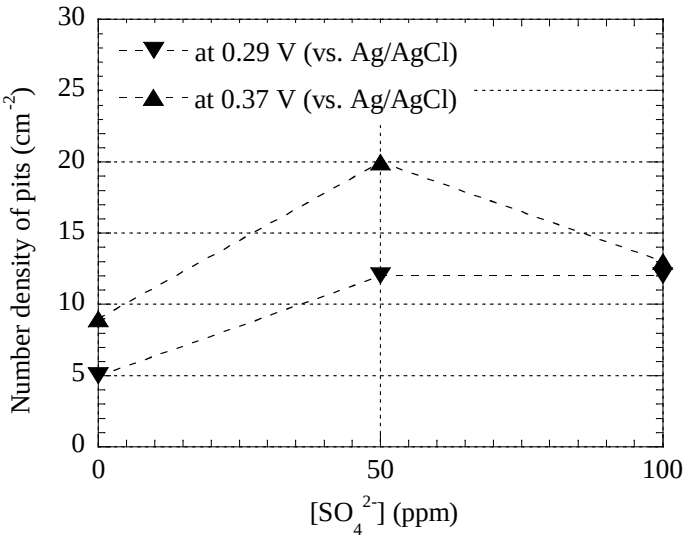


**Fig. 8.** Number density of pits on the specimens after potentiostatic polarization in the test waters for 20 h.

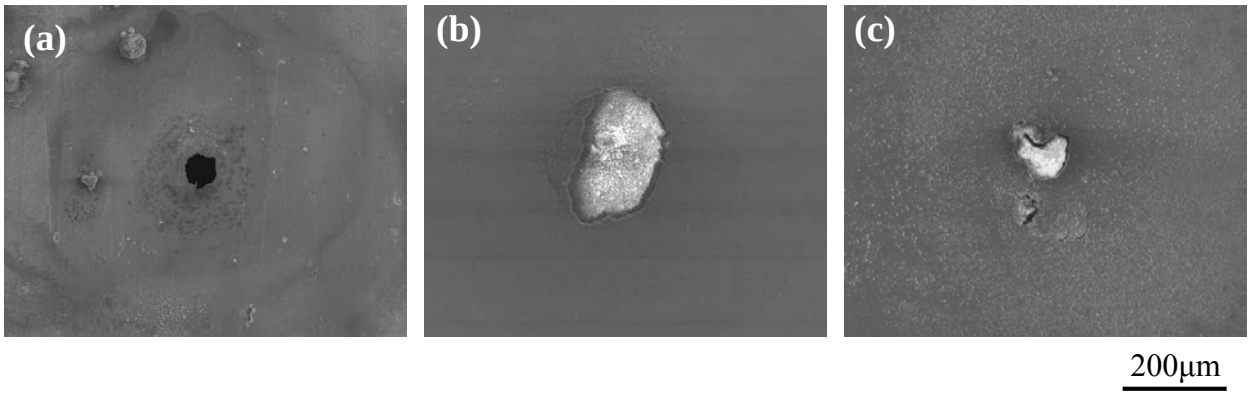


**Fig. 9.** Typical pits on specimens after potentiostatic polarization at 0.29 V (vs. Ag/AgCl) in simulated AVT waters with (a) 100 ppm $Cl^-$, (b) 100 ppm $Cl^-$ + 50 ppm $SO_4^{2-}$, and (c) 100 ppm $Cl^-$ + 100 ppm $SO_4^{2-}$.

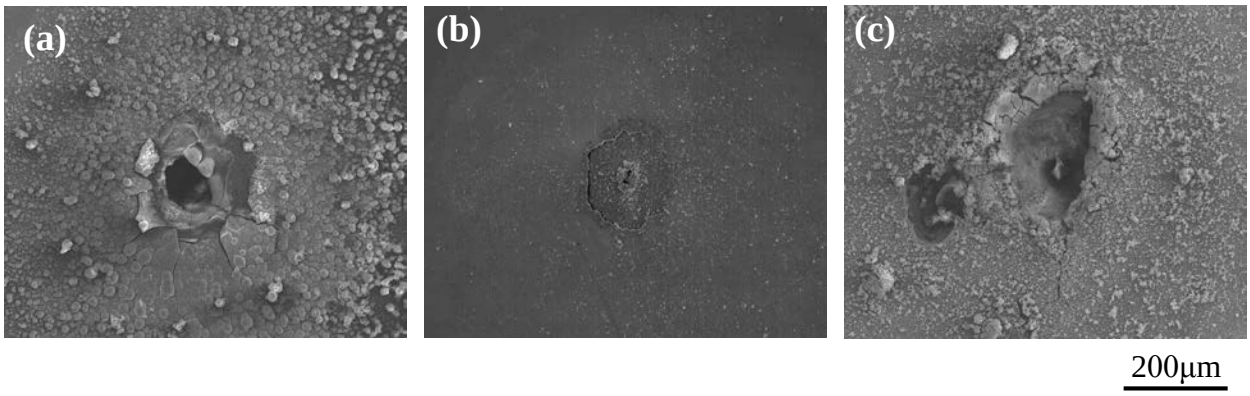


**Fig. 10.** Typical pits on specimens after potentiostatic polarization at 0.37 V (vs. Ag/AgCl) in simulated AVT waters with (a) 100 ppm $Cl^-$, (b) 100 ppm $Cl^-$ + 50 ppm $SO_4^{2-}$, and (c) 100 ppm $Cl^-$ + 100 ppm $SO_4^{2-}$.

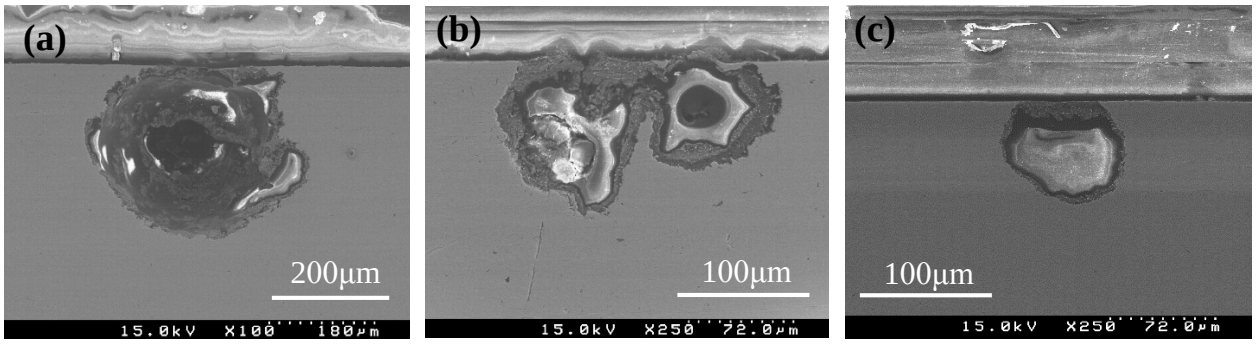


**Fig. 11.** Cross-sectional SEM images of the pits on specimens after potentiostatic polarization at 0.29 V (vs. Ag/AgCl) in simulated AVT waters with (a) 100 ppm $Cl^-$, (b) 100 ppm $Cl^-$ + 50 ppm $SO_4^{2-}$, and (c) 100 ppm $Cl^-$ + 100 ppm $SO_4^{2-}$.

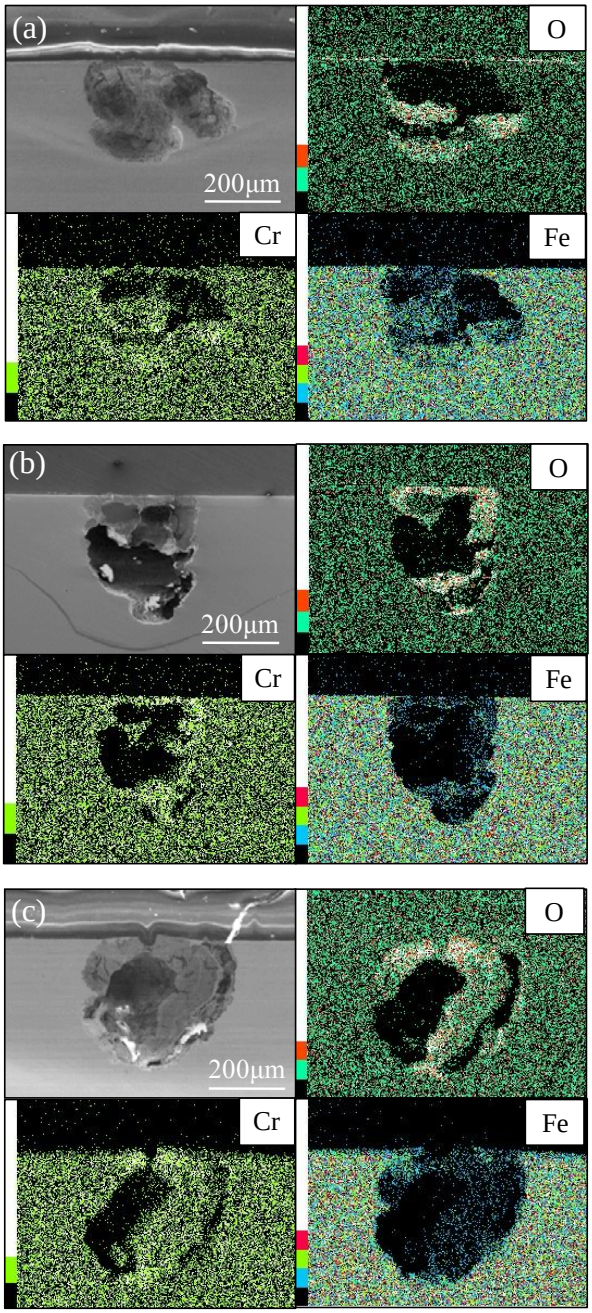


**Fig. 12.** SEM images and elemental maps of pit cross-sections on specimen surfaces after potentiostatic polarization at 0.37 V (vs. Ag/AgCl) in simulated AVT waters with (a) 100 ppm $Cl^-$, (b) 100 ppm $Cl^-$ + 50 ppm $SO_4^{2-}$, and (c) 100 ppm $Cl^-$ + 100 ppm $SO_4^{2-}$.

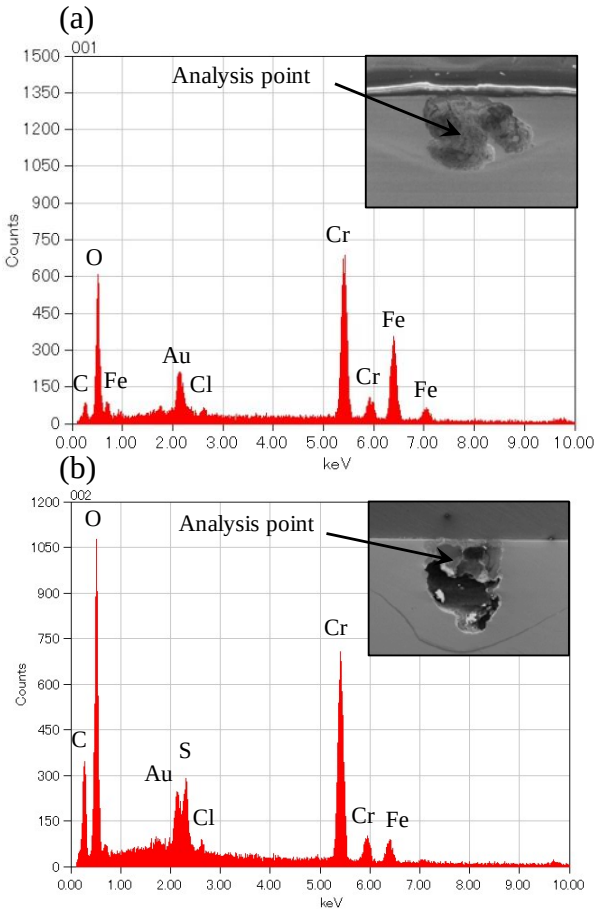


**Fig. 13.** EDS spectra for the inner surfaces of pits on specimens after potentiostatic polarization at 0.37 V (vs. Ag/AgCl) in simulated AVT waters with (a) 100 ppm $Cl^-$ and (b) 100 ppm $Cl^-$ + 50 ppm $SO_4^{2-}$. (C and Au detected are due to the Au-sputtering treatment.)